J. Biophotonics 7, No. 5, 332–340 (2012) / DOI 10.1002/jbio.201200173

Journal of BIOPHOTONICS

FULL ARTICLE

Coupled external cavity photonic crystal enhanced fluorescence

Anusha Pokhriyal[1], *Meng Lu*[2], *Chun Ge*[2], *and Brian T. Cunningham*[*,2,3]

[1] Department of Physics, University of Illinois, Urbana-Champaign, USA
[2] Department of Electrical and Computer Engineering, University of Illinois, Urbana-Champaign, USA
[3] Department of Bioengineering, University of Illinois, Urbana-Champaign, USA

Received 31 August 2012, accepted 22 September 2012
Published online 8 November 2012

Key words: photonic crystal, fluorescence enhancement, external-cavity laser, nanostructured surface

Supporting information for this article is available free of charge under http://dx.doi.org/10.1002/jbio.201200173

We report a fundamentally new approach to enhance fluorescence in which surface adsorbed fluorophore-tagged biomolecules are excited on a photonic crystal surface that functions as a narrow bandwidth and tunable mirror of an external cavity laser. This scheme leads to ~10× increase in the electromagnetic enhancement factor compared to ordinary photonic crystal enhanced fluorescence. In our experiments, the cavity automatically tunes its lasing wavelength to the resonance wavelength of the photonic crystal, ensuring optimal on-resonance coupling even in the presence of variable device parameters and variations in the density of surface-adsorbed capture molecules. We achieve ~10^5× improvement in the limit of detection of a fluorophore-tagged protein compared to its detection on an unpatterned glass substrate. The enhanced fluorescence signal and easy optical alignment make cavity-coupled photonic crystals a viable approach for further reducing detection limits of optically-excited light emitters that are used in biological assays.

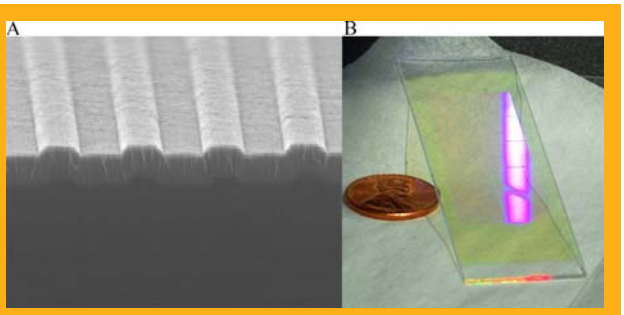

Cross-sectional SEM of the PC fabricated by nanoimprint lithography and image of the device after fabrication.

1. Introduction

Surface-based fluorescence assays have become a mainstay of molecular diagnostics [1, 2] gene expression analysis [3, 4], several next-generation DNA sequencing platforms [5–7], and cell microscopy [8]. All fluorescent assays would benefit from greater signal-to-noise ratios, which enable detection of disease biomarkers at lower concentrations in serum for earlier disease diagnosis, and detection of genes that are expressed at the lowest levels. Likewise, improvement in the efficiency of fluorescence excitation and the efficiency of emission photon collection can enable detection instrumentation to utilize miniature, low power laser sources and inexpensive uncooled imaging cameras, which would result in portable, low-cost detection systems that can be used in clinical settings.

* Corresponding author: e-mail: bcunning@illinois.edu

While fluorescence assays are typically performed upon low-autofluorescence glass or plastic surfaces, a variety of nanostructured optical surfaces have demonstrated the ability to increase the detected photon output through the mechanisms of enhanced excitation, directional emission and reduced fluorescence lifetimes [9–13]. Such structures include plasmonic gratings, nanoantennas, and photonic crystals (PC) [14–17], which are each capable, to varying degrees, of efficiently coupling incident light from a laser into surface-confined resonant electric fields (enhanced excitation), while at the same time directing fluorescence emission in a direction normal to the surface for increased collection efficiency of the detection instrument's optics (enhanced extraction). PCs have been shown to be especially advantageous because their periodic dielectric structures are comprised of materials without loss at the critical wavelengths, and thus provide high quality factor (Q-factor) resonances that, in turn, generate strongly confined electric fields near the PC surface. Because PCs are not comprised of metals that are known to quench fluorescence, fluorophores may be placed within the region of greatest electric field intensity while still maintaining high quantum efficiency [18–20]. The combined effects of enhanced excitation and enhanced extraction are multiplicative, resulting in improvements in measured detection limits by two orders of magnitude [21].

Every previous report of fluorescence enhancement has operated through simple illumination of the nanostructured surface with a laser, which often requires illumination with a specific combination of wavelength and incident angle to generate strong surface coupling. In this work, we demonstrate a fundamentally new approach that is capable of generating an even greater enhanced excitation effect, in which the PC itself serves as a tunable mirror of an external cavity laser (ECL). ECLs are generally comprised of a source of optical gain, such as a diode or semiconductor optical amplifier, that establishes a resonant optical cavity with a reflective surface that is spatially separated from the gain source. While PCs have been used previously as a mirror of an ECL [22], it has not been recognized that such a configuration leads to even higher evanescent fields on the surface of the PC that can be used for purposes of coupling energy to surface-adsorbed light emitters. Such an approach will not only benefit fluorescence detection, as demonstrated here, but can also be applied to enhancement of surface-enhanced Raman spectroscopy when it is performed upon a PC surface [23].

Here, we utilize an antireflection-coated semiconductor laser diode (LD) with a gain spectrum in the $639 < \lambda < 645$ nm wavelength region as the optical pump source of an ECL with a PC surface as the external mirror. As shown schematically in Figure 1A,

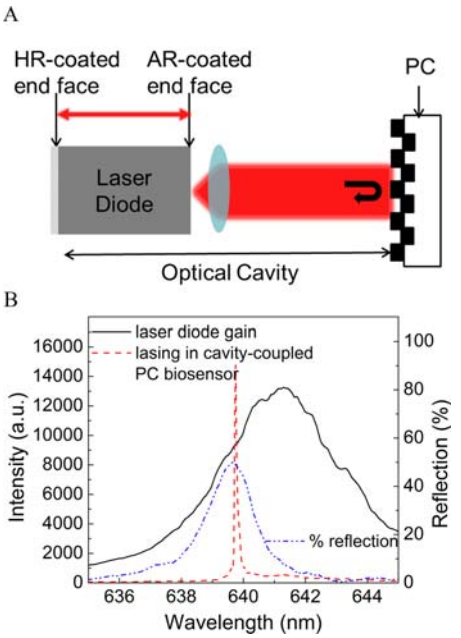

Figure 1 Working principle of external cavity coupled photonic crystal enhanced fluorescence. (**A**) The resonantly reflected laser wavelength from the PC provides feedback to the diode. The cavity then lases at the resonant wavelength of the PC. Addition of biomolecules to the surface of the PC shifts the resonant reflected wavelength, which in turns changes the lasing wavelength of the PC. (**B**) Overlap of resonantly reflected laser by the PC and the gain of the diode with the modes of the cavity determine the lasing wavelength of the cavity.

the PC is designed to perform as a narrow bandwidth resonant reflectance filter with a peak reflectance wavelength that falls within the LD gain spectrum. The lasing wavelength of the ECL cavity is selected by the peak reflectance wavelength of the PC, and is tuned by the adsorption of biomolecular layers upon the PC surface. Chemical fluorescent dyes and semiconductor quantum dots are selected with strong absorption at the lasing wavelength, and are excited by surface-confined electric field standing waves that occur on the PC. Our experimental demonstrations are supported by a theoretical investigation on the working principle of this cavity-coupled PC using finite-difference time domain (FDTD) electromagnetic modeling. The model is used to study the electric field distribution that develops on the PC surface with the optical feedback. Compared to the PC without feedback from the laser, the PC in the ECL configuration shows increased surface electromagnetic fields, which in turn provide enhanced illumination intensity to surface-bound fluorophores.

Using PCs fabricated upon quartz substrates by nanoimprint lithography, we experimentally demon-

strate that this cavity-coupled PC configuration results in a 10× stronger evanescent field upon the surface of the PC compared to the field on the PC substrate without a feedback cavity. Upon comparison of the net signal intensity from fluorescence molecules within the PC-ECL configuration to the signal obtained on an unpatterned glass surface, an enhancement factor of ~360× is observed. Direct application of dye-labeled protein to the surfaces of PCs over a range of protein concentrations is used to demonstrate that use of the PC-ECL system provides a 10^5× advantage in Limit of Detection (LOD) compared to detection upon a glass substrate. We further demonstrate that the PC-ECL configuration will tune itself to the resonant wavelength of the PC, thus eliminating the need to adjust the incident angle of the detection instrument when the PC is altered by surface chemistry layers or by capture molecules. Our results show that integration of photonic crystal enhanced fluorescence (PCEF) with excitation via an external cavity provides efficient coupling from the illumination source and greater enhanced excitation than an equivalent system that operates without the benefit of optical feedback.

2. Results

2.1 Cavity-coupled photonic crystal for fluorescence enhancement

Figure 1A shows the working principle of the cavity-coupled PC-ECL system, which is comprised of a laser diode (LD), the PC, and a system for detecting fluorescence output as either an intensity output or an image. One facet of the LD has high reflectance (95%) while the other facet is coated with an anti-reflection layer (reflectance $R < 10^{-4}$). The PC surface is placed directly in front of the AR-coated facet, with a lens between them to collimate the light onto the PC, and to focus the reflection back into the diode. The PC is designed to have a reflection resonance wavelength within a $639 < \lambda < 645$ nm range, to overlap with the gain spectrum of the LD. The PC couples to the modes of this external cavity and provides feedback to the LD. When the PC resonance matches the optical cavity modes lying within the gain spectrum of the diode, the entire cavity lases with single mode output spectra as shown in Figure 1B.

As described in previously reported detection instruments that take advantage of PCEF, variability in the PC will lead to variability in the precise incident angle required to produce resonant coupling for a fixed wavelength, which in turn necessitates precise tuning of the incident angle in order for the surface to be maintained on-resonance [24]. The PC-ECL configuration eliminates this constraint. As the cavity only lases with the feedback from the PC, the lasing wavelength always corresponds to the PC resonance wavelength. The self-tuning action is shown in Figure 2A, for several discrete positions on the PC surface, where a slight gradient in the TiO_2 film thickness results in a gradient in resonant wavelength across the device. It can be seen that with feedback the lasing wavelength corresponds to the peak in the reflection spectrum of the PC. This self-tuning ability of the PC-ECL configuration is useful for efficient excitation of surface-bound fluorophores, as adsorption of capture molecules and other surface chemistry layers also shift the resonant coupling condition of the PC. The adsorption of biomolecules to the surface of the PC increases the effective refractive index of the resonant mode, which in turn shifts the resonant wavelength of the PC to a longer wavelength. We observe that a positive shift in the resonant reflection wavelength of the PC caused by biomolecule adsorption in turn causes a positive shift of the lasing wavelength of the ECL.

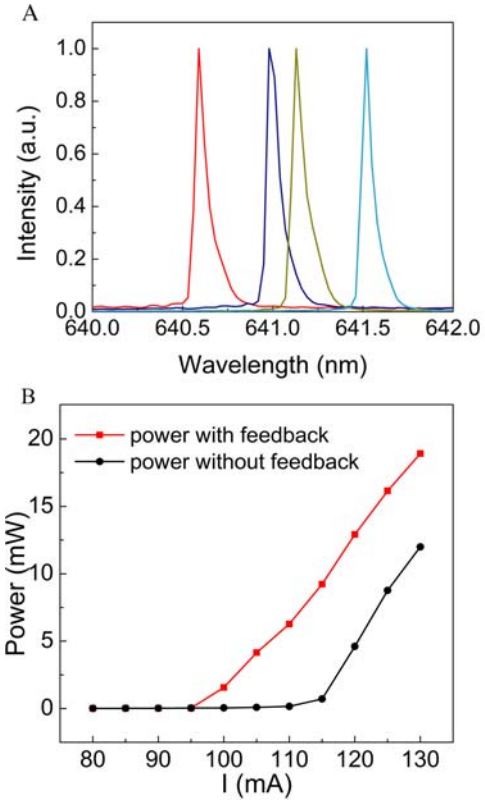

Figure 2 Self tuning and cavity laser power. (**A**) Change in the resonant reflection wavelength of the PC shifts the lasing wavelength of the cavity. (**B**) The laser power incident on the PC surface with and without coupling to the cavity, demonstrating that the PC feedback reduces the lasing threshold.

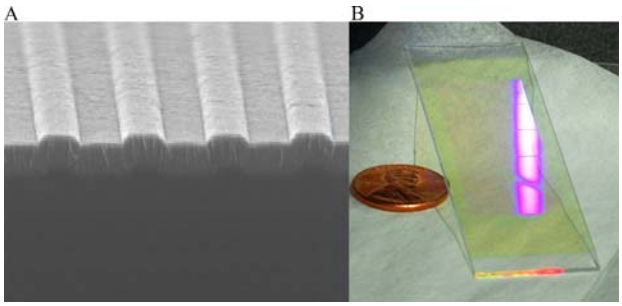

Figure 3 Device design. (**A**) Cross-sectional SEM of the PC fabricated by nanoimprint lithography. (**B**) Image of the device after fabrication.

As a result, a surface-bound fluorophore is always excited with the PC in an optimal on-resonance condition. While the diode is capable of lasing without feedback from the PC, its interaction with the PC through the formation of an external cavity effectively reduces the lasing threshold. This effect is clearly observed in Figure 2B, which shows the emitted power with feedback and without feedback for equal diode injection current. The self-tuning behavior is only observed when feedback from the PC is present.

As shown in Figure 3, the PC is fabricated on a quartz substrate selected for its low autofluorescence (See Methods) [21]. The PC structure is comprised of a periodic ($\Lambda = 400$ nm) linear grating structure that is patterned by nanoimprint lithography and etched into the quartz by reactive ion etching (depth, $d = 40$ nm). After removal of the imprint resist, the quartz grating is coated with a film of TiO_2 by sputtering to complete the structure (thickness, $t = 125$ nm). The PC period, grating depth, and TiO_2 thickness are selected to produce a surface that resonantly reflects a narrow band of wavelengths that falls within the gain spectrum of the diode when the media above the PC is comprised of air. The width of the lasing peak and the suppression of the sidebands in the lasing profile depend largely upon the reflectivity and the linewidth of the reflection peak of the PC [25]. In previous work, we have shown that an optimal design for PC enhanced fluorescence utilizes transverse magnetic (TM) polarized light (polarization perpendicular to grating direction) for normal excitation and transverse-electric (TE) polarized light (polarization parallel to grating direction) for extraction of the emitted fluorescence signal [26]. Therefore, the PC was designed for normal-incidence excitation using TM polarized light to have a resonance in the $639 < \lambda < 645$ nm wavelength range.

FDTD simulations were performed to model the coupling between the optical cavity and the PC, using a simplified approach that approximates the behavior of the actual external cavity. Figure 4A shows a schematic of the simulated FDTD model. The simulation space must be partitioned into small volume elements with a size scale that can accurately

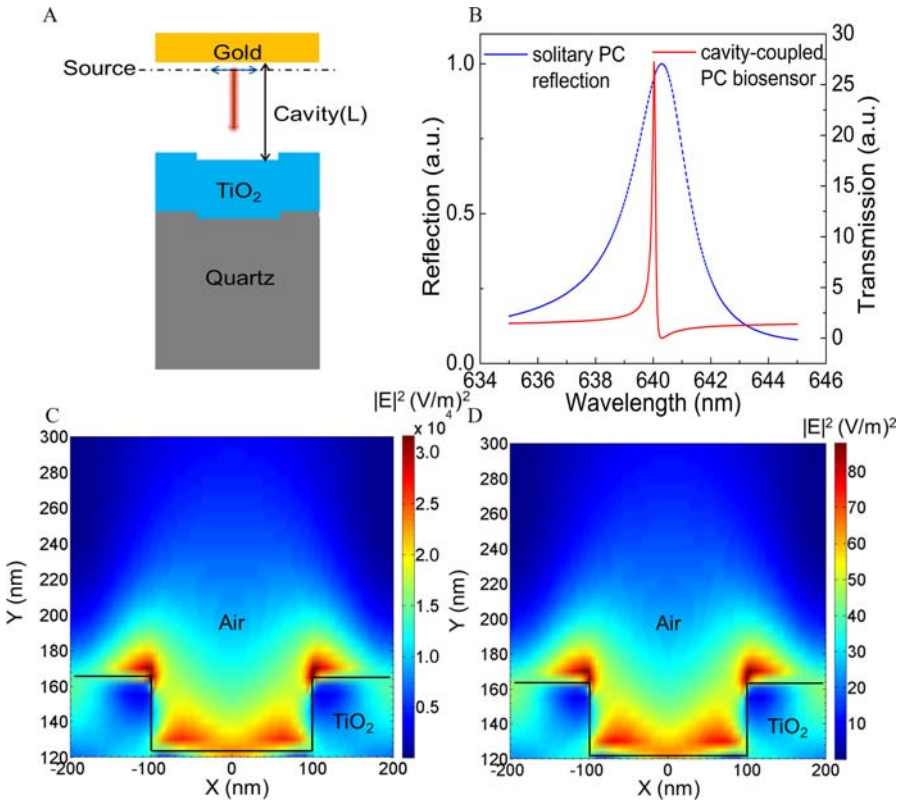

Figure 4 Theoretical formulation. (**A**) Schematic illustration of a unit cell simulated using FDTD, showing one period of the PC and a plane-wave source sandwiched between the PC and a gold mirror for a cavity of length *l*. (**B**) FDTD computed far-field transmission intensity for PC-coupled cavity showing cavity modes enveloped by a PC resonance mode. The peak in the transmission spectrum represents lasing action in the cavity. (**C**) Simulated electric field intensity on the PC surface when coupled to the cavity. (**D**) Simulated electric field intensity on the PC surface when incident light is resonantly coupled to the PC. On averaging the field in 5nm area above the PC surface (for both c–d), an increase of 330× in the average fields is calculated for the cavity-coupled PC biosensor.

capture the spatial variability of electromagnetic fields near the PC surface. If a spatial dimension of 5 nm for such a cell were used, the entire length of the cavity (30 cm) would be too large to be easily simulated. Because the vast majority of the cavity is comprised of empty space, we chose to simulate a shorter cavity (1.85 μm) that produces the same physical effect, with the exception of the wavelength spacing between allowed external cavity modes, as described by the free spectral range (FSR),

$$\mathrm{FSR} = \frac{\lambda_0^2}{2nl\cos\theta + \lambda_0} \quad (1)$$

where n is the refractive index of the cavity, l is the length of the cavity, θ is the angle of incidence and λ_0 is the central wavelength of the nearest transmission peak.

For our 30 cm external cavity, the spacing between the optical modes is FSR ~0.7 pm, ensuring that the PC resonance peak always overlaps with an available cavity mode that provides feedback to the diode. Within the simulation, the laser diode was replaced by 200 nm thick gold to act as the high reflectivity end of the cavity. A TM polarized plane wave source (overlapping a wavelength range of $639 < \lambda < 645$ nm) was inserted into the cavity. When the PC is not coupled to the cavity, its simulated resonant reflection displays a full-width at half-maximum (FWHM) of ~2 nm, as shown in Figure 4B, which is also observed experimentally, as shown in Figure 1B. Insertion of the PC into the cavity results in narrowing of the resonant transmission spectrum to FWHM = 0.1 nm (Figure 4B). This phenomenon is also experimentally observed (Figure 1B) as the stimulated emission in the diode, and combined with feedback, results in lasing of the external cavity system.

Importantly, the interaction of the PC with the external cavity results in an increased evanescent electric field magnitude on the surface of the PC, thus providing an additional mechanism for PCEF gain. Figure 4C–D compare the simulated power density ($|\mathbf{E}|^2$) associated with the electric field near the surface of the PC for the PC-ECL configuration, compared to a PC that is resonantly excited by the illumination source without the benefit of an external cavity. Averaging $|\mathbf{E}|^2$ within the volume of media that is within 5 nm of the sensor surface (within the air media), where surface-bound fluorophores would be located, an enhancement factor of 330× is obtained. Our simulation supports the hypothesis that evanescent fields with enhanced magnitude will form upon the PC surface within the cavity, and lead to efficient enhanced excitation of surface-adsorbed light emitters, such as fluorophores and quantum dots. The simulation utilizes uniform perfect plane waves and a cavity that does not suffer from various sources of optical loss; therefore we expect experimental enhancements to not be as high as in simulation.

2.2 *Enhanced excitation of quantum dots and dye-labeled streptavidin*

To demonstrate enhanced excitation of fluorophores by the cavity-coupled PC, detection experiments were performed using streptavidin labeled with a fluorescent dye (Alexa633), and semiconductor quantum dots (QD) coated with streptavidin. A schematic diagram of our detection instrument is shown in Figure 5, which enables us to gather fluorescent images of the PC surface from below the substrate, while the cavity is formed above the substrate. An excitation filter was added to the cavity to attenuate laser diode emission at wavelengths greater than $\lambda = 650$ nm, while a quartz window was added to monitor the power inside the cavity at one end, while enabling measurement of the lasing spectrum at the other end. For the 1-dimensional PC, the resonance coupling condition only depends upon the angle between the incident beam and the grating's normal vector in the plane perpendicular to grating direction (labeled as θ in Figure 5). The resonance condition is insensitive to the angle in the plane along the grating direction (ϕ). The diode illumination was incident on the PC at an angle of $\theta = 0°$ and $\phi = 17°$. This configuration ensures that no excitation light leaks into the objective (NA = 0.28, acceptance angle ~16°) of the imaging setup, thus reducing background noise in our collected signal while the resonance condition for the PC is maintained. The resonantly reflected light from the PC

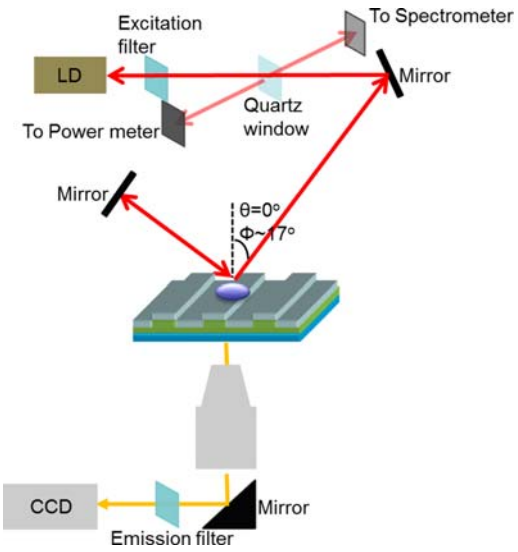

Figure 5 Detection instrument schematic. Cavity-coupled PC with the imaging setup used in the experiment. A resonance angle of $\theta = 0°$ is used as the incidence angle for the laser on the PC. $\phi = 17°$ is chosen to prevent the transmitted laser light from entering the objective.

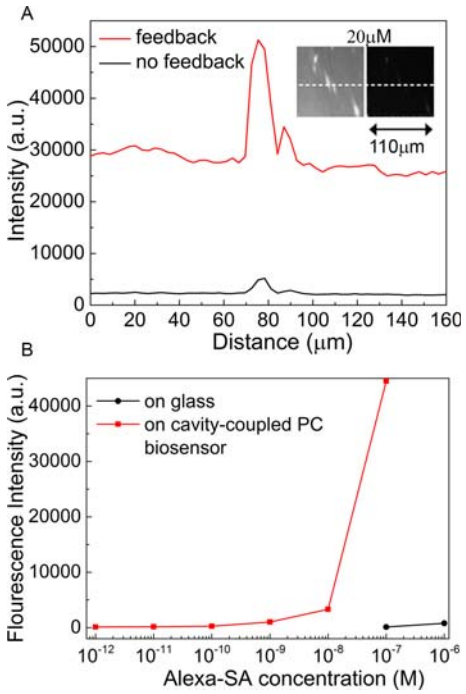

Figure 6 Fluorescence enhancement. (**A**) (Inset) Fluorescence images of quantum dot labeled streptavidin on a solitary PC and a PC-coupled cavity. Line profile of the images showing an enhancement of 10×. (**B**) Plot of net fluorescence signal intensity of Alexa-streptavidin versus its concentration to compare the signal intensity from the PC-coupled cavity biosensor and glass. The limit of detection on the PC was ~1 pM compared to an unpatterned glass surface, where no spots were seen below 0.1 μM.

retraces its path back to the diode by reflection against a mirror, thus forming the cavity.

To compare the evanescent field magnitude on the surface of the PC in the cavity to its magnitude without the cavity, while avoiding the effects of photobleaching, streptavidin-coated QDs selected for their absorption at $\lambda = 640$ nm were used (QD 705, Life Technologies, emission wavelength = 705 nm). The streptavidin-coated QDs were applied using a pipette at a concentration of 20 μM on a PC surface that had been functionalized with dimethylethoxysilane. After an overnight incubation and a wash with deionized water, fluorescence intensity was measured with the PC on-resonance and with the cavity-coupled PC at the same incident laser power. This was achieved by blocking and unblocking the resonantly reflected laser beam from reaching the second mirror and adjusting the injection current to the diode. The net fluorescence intensity (emission-background fluorescence) on the cavity-coupled PC was increased by a factor of 10×, compared to the solitary PC, as shown in Figure 6A. No measureable increase in the background and noise were detected in the cavity-coupled PC compared to PCEF giving an increase in signal-to-noise ratio (*S/N*) of 10×. This factor represents the gain achieved over "ordinary" PCEF.

To demonstrate the overall gain for this approach compared to detection of the same analyte on an ordinary glass surface, we tested a series of concentrations (1 μM–1 pM range) of Alexa-633 labeled streptavidin (Alexa-SA). The net fluorescence signal intensity of Alexa-SA on the PC surface substantially increased for all concentrations tested, compared to the signals from the glass surface (Figure 6B). These measurements were taken using identical incident laser power, camera gain, and integration time. The highest concentration of Alexa-SA on the cavity-coupled PC resulted in saturation of the photon count available from the CCD. On the glass surface, only the two highest Alexa-SA concentrations were visible, while all lower concentrations resulted in fluorescence counts lower than the background noise level. The concentration of 1 pM was observed on the cavity-coupled PC biosensor with a signal-to-noise ratio (*S/N*) of ~6.1, while no fluorescence was detected on the glass surface for concentrations below 0.1 μM. As the concentration was increased, fluorescence intensity on the cavity-coupled PC increased while the signal intensity on the glass surface only started to show a detectable signal starting above 0.1 μM (an intensity equivalent to the 1 pM concentration on the cavity-coupled PC). For the concentrations of Alexa-SA that were measurable upon both the PC and the glass surface, comparison of the net signal intensity demonstrated an enhancement factor of ~360×.

3. Discussion

In this work, we demonstrated for the first time that a PC surface excited within an optical cavity results in enhanced fluorescence with even greater evanescent field magnitude than is available from an equivalent surface that is illuminated by ordinary laser exposure. The higher magnitude evanescent electric fields generated by this method have been shown theoretically and experimentally to reduce achievable limits of detection and to increase signal-to-noise ratio for two varieties of optically pumped light emitters, namely chemical fluorophores and semiconductor quantum dots.

We envision PC-ECL excitation to be applicable to any surface-based fluorescence bioassay that is currently performed upon a glass surface, particularly those that would benefit from reduction of detection limits, or development of a miniature detection instrument for clinical point-of-care applications. For example, "sandwich" assays for detection of disease biomarkers in serum utilize fluorophore-tagged secondary antibodies to specifically label cap-

tured analytes [27], but achieve detection limits that are typically two orders of magnitude lower than the dissociation constant for the interaction of the capture antibody and the analyte. PCEF has demonstrated the ability to enhance weak fluorescence signals for low concentration biomarkers, thereby reducing detection limits [28] and potentially achieving the ability to perform diagnosis at an earlier stage. Further increase in the electromagnetic enhancement factor will enable the detection limits achievable via PCEF to be pushed further.

An important aspect of the detection system is its throughput, as measured by its ability to integrate a large number of biological assays into a small PC surface area. The most basic implementation of a PC-ECL instrument, illuminates a ~2200 μm^2 region of the PC with a collimated (but not focused) laser beam and measures fluorescence intensity integrated from that entire region, essentially performing one assay with a single illuminated spot. Such an approach will be appropriate to assays performed within standard format microplate wells, in which the entire bottom surface of each well would be covered with PC, and coated with a uniform layer of capture molecules. We also envision, as partially demonstrated here, the ability to capture fluorescent images of the PC surface while it is being excited by the external cavity, which would enable a PC surface to be partitioned into a microarray of discrete capture spots. We have observed that an important factor that must be addressed for the PC-ECL approach to become effective for imaging is to achieve a high level of illumination uniformity. In the implementation of the system presented here, the diode illuminates a ~700 μm diameter region with a Gaussian beam, resulting in only a ~2200 μm^2 region in the center of the beam experiencing strong excitation. To overcome this limitation, we envision an illumination approach in which the beam will be focused by a cylindrical lens with its cone of incident angles spread in the ϕ direction, while the orthogonal θ direction couples to the PC in the on-resonance condition [29]. Such an approach would allow a fluorescent image to be gathered for a tightly focused line, which would then be scanned across the PC to gather an image of an entire surface populated with small capture spots. Such an imaging approach could be extended to detection of other surface-bound fluorescent emitters, such as those used to label the surface of cells or tissue. We further expect this approach to translate to PC structures operating within a microfluidic channel, enabling enhanced detection of analytes (such as virus particles or DNA molecular beacons) flowing through the channel and entering the evanescent field region of the PC [30].

Besides enhancing fluorescence, the cavity-coupled PC may also be employed to further magnify surface enhanced Raman spectroscopy (SERS). As SERS signal scales with $|\mathbf{E}|^4$, any increase in $|\mathbf{E}|$ would lead to considerable increase in the signal. Thus SERS signal of a molecule linked to metal nanoparticles dispersed on the surface of the PC can be enhanced by overlapping the extinction spectra of the particle with the resonance of the cavity-coupled PC. The optical gain provided by the diode in this case can help overcome sources of optical loss/absorption from metal nanoparticles while enhancing the coupling of the laser to the metal nanoparticle via PC. We expect this to be a topic of future work.

To conclude, we have presented a novel method, supported by experimental demonstrations and theoretical modeling, for sensitive detection of dye-labeled proteins in which a PC surface serves as a tunable mirror of an external cavity laser, where the cavity results in an enhanced evanescent field magnitude above that generated by ordinary PCEF. In addition to greater sensitivity, the approach provides a self-tuning capability that ensures on-resonance excitation of the cavity, even as the PC resonant condition is altered by attached biomolecules. Using both chemical fluorophores and semiconductor quantum dots, we demonstrate detection limits over ~10^5-fold lower than traditional techniques. Coupled with the simplicity afforded by physical signal enhancement and compatibility with existing biodetection tools, the cavity-coupled PC is expected to find broad use in disease diagnosis and other fluorescence-based sensing applications.

4. Methods

4.1 PC fabrication

The PC was fabricated using the step and flash nanoimprint lithography technique, using a Molecular Imprints Imprio-55 tool. Briefly, a quartz template was fabricated (Dai Nippon Printing Co., Ltd.) with a linear grating structure (period = 400 nm, depth = 100 nm, 50% duty cycle) by e-beam lithography with a grating area of 9×9 mm. A 4-inch quartz wafer was used as a substrate for the PC. A planarization layer (Transpin, Molecular Imprints) was spin-coated onto the wafer prior to dispensing droplets of the imprint resist (MonoMat, Molecular Imprints) so as to fill the template pattern without extrusions. The template was pretreated with a release layer (RelMat, Molecular Imprints) and was pressed onto the imprint resist creating a replica of the mold. The imprint resist was cured into a solid phase by exposure to ultraviolet light. The template imprint/cure/release process was stepped and repeated across the wafer to create a 4×7 array of

gratings. A resist (Silspin, Molecular Imprints) was then spin coated over the imprint resist, to serve as a hard mask for the etching process. Reactive-ion etching was then used to transfer the pattern onto the wafer surface with a depth of 40 nm. After removal of the resist films and planarizing films (using Piranha clean), TiO_2 (~125 nm, refractive index ~2.35) was sputtered onto the wafer. Finally, the wafer was diced to produce 2, 1×3 in^2 slides.

4.2 FDTD model

Here we used FDTD (Lumerical FDTD, Vacouver, Canada) to model the coupling between the optical cavity and the PC, using a simplified approach that approximates the behavior of the actual external cavity. The detailed FDTD model of the simulated structure appears in supplementary Figure S1 where the cavity lengths, gold mirror, source position, grating period, grating depth and TiO_2 thickness are L, M, h, Λ, d and t, respectively. The refractive indices of gold and Quartz were taken from the material database of Lumerical; CRC for gold and SiO_2 (Palik) for Quartz. The refractive index of TiO_2 was taken as 2.35 for all the wavelengths used in the simulation. The structure was excited by a linearly polarized (TM), plane-wave with the wavelength range overlapping $639 < \lambda < 645$ nm. The PC was designed to have a reflection resonance within $639 < \lambda < 645$ nm, by tuning the thickness of TiO_2 deposited on the grating surface. A 200 nm thick gold mirror replaced the LD. Periodic boundary conditions were chosen along the grating and PML on the top and bottom surfaces of the simulation region. An accuracy of at least $\lambda/22$ was used within the simulation region with mesh size of 5 nm in the region of the PC. The shorter cavity simulated here produces the same effect as a longer cavity except for the spacing between the optical cavity modes. In order to ensure that at least one optical mode of the external cavity couples to the PC, a simulation was performed for various cavity lengths. Supplementary Figure S2 plots the transmitted intensity from the bottom of the PC for different cavity lengths for a range of wavelengths. From this data, a cavity length of 1.85 μm was chosen, for which one of the optical modes coupled to the PC mode. A cross-section of the transmission efficiency at the cavity length of 1.85 μm is shown in Figure 4B. The evanescent field profile on the PC surface was then generated at this transmission peak wavelength and is shown in Figure 4C. The cavity-coupled PC was then compared to PC without a cavity. For this comparison, the PC in Figure S1 was simulated without the gold mirror, while the remaining simulation parameters were kept constant. Figure 4B compared this PC reflection peak to the cavity-coupled PC. The evanescent field profile on the PC surface generated at this reflection peak wavelength is shown in Figure 4D.

4.3. Far-field transmission measurements

Transmission spectra were collected by a fiber-coupled collimating lens with its distal end connected to a spectrometer with a wavelength resolution of 0.06 nm (Ocean Optics HR 4000).

4.4. Dye-labeled detection experiments

The Alexa-SA (streptavidin, alexa fluro 633 conjugate, Invitrogen) and quantum dot-SA (Qdot 705 streptavidin conjugate, Invitrogen) solutions were prepared in 1 × Phosphate-buffered saline (PBS) solution, pH = 7.4. The surfaces used in the experiment were cleaned and functionalized using dimethylethoxysilane by an overnight incubation in a vacuum chamber heated to a temperature of 80 °C. The slides were then washed in toluene, methanol, and de-ionized (DI) water to rinse off any excess silane. The Alexa-SA and quantum dot-SA solutions were deposited in the form of a ~1 mm diameter droplet on the samples using a precision pipette (± 5% accuracy at 1 μL). The samples were then incubated overnight and then washed and dried in PBS-tween and DI before taking fluorescence measurements.

4.5 Fluorescence measurements

The LD (Ridge Waveguide Laser Diode, SAL-640–100, Sacher Lasertechnik) illuminates a ~700 μm diameter spot on the PC surface. The incident laser power in the cavity was monitored using a power meter and controlled using a diode injection current controller (E3620A, Agilent). All the images were taken using a laser power of 2 mW incident on the substrate both with and without feedback. A 10× objective (NA = 0.28) was used to collect the fluorescence signal, which was then imaged by an EMCCD (Cascade 512B) with a field of view of 800×800 μm^2. An integration time of 30 ms was used for all the images along with the multiplication gain of 3000. A long pass emission filter ($\lambda > 664$ nm, SEMROCK-BLP01–664R-25) was used to block any excitation light leaking into the objective. The net intensity for all the fluorophores was calculated by subtracting the background substrate fluorescence from the fluorophore emission.

Acknowledgements This work was supported by National Science Foundation (CBET11–32225) and the National Institutes of Health (R01 GM086382). Any opinions, findings, and conclusions or recommendations expressed in this material are those of the authors and do not necessarily reflect the views of the National Science Foundation.

Author contributions A. P., M. L., C. G. conceived the experiments. A. P. designed and performed the experiments and analyzed the simulated data. B. T. C. provided guidance. A. P. and B. T. C. co-wrote the paper.

Conflict of interest The authors declare no competing financial interests.

Author biographies Please see Supporting Information online.

References

[1] H. Jin and R. C. Zanger, Cancer Biomarkers **6**, 281–290 (2010).
[2] G. MacBeath and S. L. Schreiber, Science **289**, 1760–1763 (2000).
[3] M. Schena, D. Shalon, R. W. Davis, and P. O. Brown, Science **270**, 467–470 (1995).
[4] S. P. A. Fodor, J. L. Read, M. C. Pirrung, L. Stryer, A. T. Lu, and D. Solas, Science **251**, 767–773 (1991).
[5] J. F. Thompson and P. M. Milos, Genome Biol. **12**, 217 (2011).
[6] F. A. Eid, J. Gray, K. Luong, J. Lyle, G. Otto, P. Peluso, D. Rank, P. Baybayan, B. Bettman, A. Bibillo, K. Bjornson, B. Chaudhuri, F. Christians, R. Cicero, S. Clark, R. Dalal, A. Dewinter, J. Dixon, M. Foquet, A. Gaertner, P. Hardenbol, C. Heiner, K. Hester, D. Holden, G. Kearns, X. Kong, R. Kuse, Y. Lacroix, S. Lin et al., Science **323**, 133–138 (2009).
[7] In Next-Generation Genome Sequencing: Towards Personalized Medicine (Wiley-VCH, Weinheim, 2008).
[8] Y. Sako, S. Minoguchi, and T. Yanagida, Nature Cell Biol. **2**, 168–172 (2000).
[9] J. R. Lakowicz, Anal. Biochem. **298**, 1–24 (2001).
[10] S. Fan and J. D. Joannopoulos, Phys. Rev. B **65**, 235112 (2002).
[11] K. A. Willets and R. P. V. Duyne, Annu. Rev. Phys. Chem. **58**, 267–297 (2006).
[12] P. Anger, P. Bharadwaj, and L. Novotny, Phys. Rev. Lett. **96**, 113002 (2006).
[13] H. Hori, K. Tawa, K. Kintaka, J. Nishii, and Y. Tatsu, Opt. Rev. **16**, 216–221 (2009).
[14] E. L. Moal, E. Fort, S. Leveque-Fort, F. P. Cordelieres, M.-P. Fontaine-Aupart, and C. Ricolleau, Biophys. J. **92**, 2150–2161 (2007).
[15] L. C. Estrada, O. E. Martinez, M. Brunstein, S. Bouchoule, L. Le-Gratiet, A. Talneau, I. Sagnes, P. Monnier, J. A. Lvenson, and A. M. Yacomotti, Opt. Express **18**, 3693–3698 (2010).
[16] A. Kinkhabwala, Z. Yu, S. Fan, Y. Avlasevich, K. Müllen, and W. E. Moerner, Nat. Photonics **3**, 654–657 (2009).
[17] K. Tawa, H. Hori, K. Kintaka, K. Kiyosue, Y. Tatsu, and J. Nishii, Opt. Express **16**, 9781–9790 (2008).
[18] S. S. Wang, R. Magnusson, and J. S. Bagby, J. Opt. Soc. Am A **7**, 1470–1474 (1990).
[19] R. Magnusson and S. S. Wang, Appl. Phys. Lett. **61**, 1022–1024 (1992).
[20] N. Ganesh, W. Zhang, P. C. Mathias, and B. T. Cunningham, Nat. Nanotechnol. **2**, 515–520 (2007).
[21] A. Pokhriyal, M. Lu, V. Chaudhery, C.-S. Huang, S. Schulz, and B. T. Cunningham, Opt. Express **18**, 24793–24808 (2010).
[22] A. S. P. Chang, H. Tan, S. Bai, W. Wu, Z. Yu, and S. Y. Chou, IEEE Photonics Technol. Lett. **19**, 1099–1101 (2007).
[23] S.-M. Kim, W. Zhang, and B. T. Cunningham, Appl. Phys. Lett. **93**, 143112–143114 (2008).
[24] V. Chaudhery, M. Lu, A. Pokhriyal, S. Schulz, and B. T. Cunningham, IEEE Sens. J. **12**, 1272–1279 (2011).
[25] S. D. Saliba, M. Junker, L. D. Turner, and R. E. Scholten, Appl. Opt. **48**, 6692–6700 (2009).
[26] P. C. Mathias, H.-Y. Wu, and B. T. Cunningham, Appl. Phys. Lett. 95, 021111–021113 (2009).
[27] S. S. R. Gonzalez, S. Varnum, and R. Zangar, High-Throughput Analysis of Serum Antigens Using Sandwich ELISAs on Microarrays (Humana Press, Totowa, NJ., 2009).
[28] P. C. Mathias, N. Ganesh, and B. T. Cunningham, Anal. Chem. **80**, 9013–9020 (2008).
[29] V. Chaudhery, M. Lu, C.-S. Huang, J. Polans, R. Tan, R. C. Zangar, and B. T. Cunningham, Opt. Lett. (accepted 2012).
[30] C. J. Choi and B. T. Cunningham, Lab. Chip. **6**, 1373–1380 (2006).

